Received 28 December 2022; revised 16 March 2023; accepted 3 April 2023. Date of publication 7 April 2023; date of current version 3 November 2023.
The review of this article was arranged by Editor K. Ota.

*Digital Object Identifier 10.1109/JEDS.2023.3265392*

# Lithium-ion-Based Resistive Devices of $LiCoO_2$/LiPON/Cu With Ultrathin Interlayers of Titanium Oxide for Neuromorphic Computing

**TAKAO MARUKAME (Member, IEEE), KOICHI MIZUSHIMA, KUMIKO NOMURA, AND YOSHIFUMI NISHI**

Frontier Research Laboratory, Nano Material and Frontier Laboratories, Corporate Research and Development Center, Toshiba Corporation, Kawasaki 212-8582, Japan

CORRESPONDING AUTHOR: T. MARUKAME (e-mail: takao.marukame@toshiba.co.jp)

**ABSTRACT** Lithium (Li)-ion materials such as $LiCoO_2$ and $(Li_3PO_4)$-N (LiPON) are used in Li-ion all-solid-state batteries, and are now expected to be used as ion-electron hybrid materials to create a new degree of freedom in future integrated circuits. We fabricated thin-film devices on the basis of $LiCoO_2$/LiPON/Cu and ultrathin titanium oxide ($TiO_x$) to demonstrate their new type of resistance change mechanism and characteristics. Multi-level resistance changes promising as synaptic plasticity were obtained, and the resistance properties enable neuromorphic computing to enter a new era.

**INDEX TERMS** Electrochemical devices, Lithium-ion batteries, memristors, neural networks, neuromorphic engineering, neuromorphics, synapses.

## I. INTRODUCTION

Artificial intelligence (AI) is used in various applications for Internet-of-Things (IoT) and automation. Because of the large size of deep neural networks (DNNs), their training, or learning, requires much computing time and effort [1], [2]. Most operations of NNs during and after training are repetitive sum-of-products operations, and graphics processing units (GPUs) are often used because they can perform these operations on a large scale and accelerate them as matrix operations. However, the drawback of GPUs is that they consume much power. Therefore, it is difficult to keep a large DNN running on a small edge device. Neuromorphic technology has shown promise as a computationally efficient hardware dedicated to AI [3], [4]. Neurons in analog circuits are simple physical networks that process information by using electrical signals, like the brain, and thus can perform highly efficient operations [5]. The technologies to mimic synapses, which are memory elements, with resistance-change materials are promising [6], [7], [8]. Materials of interest for resistance change elements include charge trap materials, phase change chalcogenide, ferroelectric materials, oxide insulators with oxygen deficiency, ion-conductive materials, and so on [9], [10], [11], [12], [13], [14], [15], [16]. Challenges for resistive devices are generally to realistically develop multi-level resistances and neuromorphic write and read sequence.

One of the most successful ion-conductive materials, not limited to the aforementioned computing applications, is lithium (Li)-ion materials because of their successful battery applications [17]. $LiCoO_2$ is widely used as a cathode material for Li-ion batteries, which provides Li ions [18]. All-solid-state batteries with Li-ions have attracted much attention for a new degree of freedom in electronics [19], [20]. Although it may be difficult to implement lithium-ion conductors directly on Si substrates, there is a good possibility to use them in 3D structures by using improved backend-of-line processes and heterogeneous wafer bonding and so on.

To fabricate all-solid-state Li-ion devices, solid oxide electrolyte is a key material to control Li-ion conductance and electron resistance. $Li_3PO_4$ and its nitride, LiPON, are a typical solid oxide electrolyte used for Li-ion based all solid-state batteries such as $LiCoO_2$/LiPON/Cu [21]. Three- and multi-terminal devices using $LiCoO_2$ as a resistive element has been reported to show a repetitive resistance change due to electrolytic transfer of Li-ions [22], [23], [24]. According to these results, ionic conduction is a promising mechanism for long-term memory and linearity of resistance change.

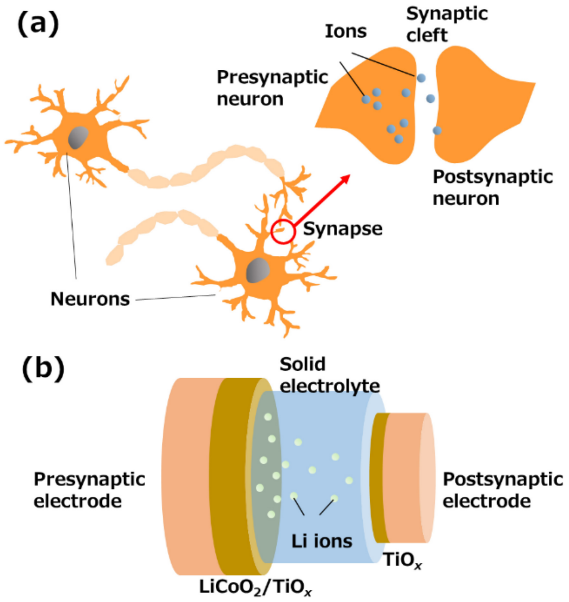


**FIGURE 1.** Ion conduction at the synapse of neurons provides information transfer and plasticity: (a) biological synapses, (b) artificial synapses using Li-ion conductions in this study.

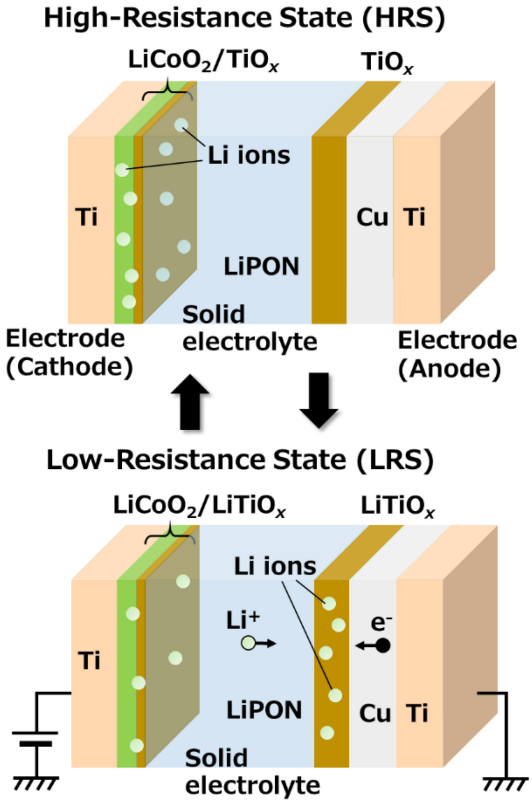


**FIGURE 2.** Mechanism of resistance change. In the initial state immediately after film deposition, the film is in a high resistance state (HRS) due to the thicker $TiO_x$; when a positive voltage is applied to the cathode side where $LiCoO_2$/thinner $TiO_x$ is present, Li-ions move to the anode and enter the thicker $TiO_x$, resulting in a low-resistance state (LRS) film of $LiTiO_x$.

However, the use of Li-ions such as thin-film all-solid-state batteries has not been demonstrated yet in integrated neuromorphic devices.

Neuromorphic engineering has utilized the charge conductivity of semiconductors and oxides rather than ionic conduction. However, the neurons of living organisms use spikes as electrical signal processing and spike-timing-dependent plasticity (STDP) [25], [26]. The mechanism of spike generation is electromotive force generation of ionized chemicals. The synaptic change mechanism responsible for memory plasticity also involves more chemical signal transduction and chemical plastic change than electrical plasticity. Figure 1 shows the relationship between neurons and synapses and the concept of a neuromorphic device with ionic conduction. A neuromorphic NN system receives inputs as spike voltages and thus uses STDP for learning, in which nonlinearity should be carefully implemented in the resistance changes [27], [28], [29], [30], [31], [32].

The purpose of this study is to design a new type of Li-ion-based device with a resistance change mechanism for neuromorphic computing and to demonstrate its resistance change properties. To clarify the resistance change characteristics of a two-terminal device using a thin-film all-solid-state battery, we inserted ultrathin layers of titanium dioxide at the interfaces and investigated the resistance change characteristics affected by pulses or spikes. Given the experimental results, we also conduct an analysis on NNs by simulations and discuss neuromorphic computing applications.

## II. DEVICE DESIGN AND EXPERIMENTAL METHODS

The operating mechanism assumed in the design phase of the Li-ion synapse device developed in this research is as follows. A schematic diagram is shown in Fig. 2, in which Li-ions move inside the device and change in a predetermined direction between a low-resistance state (LRS) in which current flows and a high-resistance state (HRS) in which current does not flow. The structure consists of an electrode such as Ti, a transition metal oxide such as $LiTiO_x$ or $LiCoO_2/TiO_x$ as a Li-ion source on the positive electrode (cathode, i.e., providing $Li^+$ ions when positively biased), a Li-ion conducting layer such as LiPON as a fundamental solid electrolyte, a transition metal oxide layer such as $TiO_x$ on the negative electrode (anode, i.e., accepting $Li^+$ ions when negatively biased), and a Cu/Ti electrode. Since $LiCoO_2$ is a conductor [18], the resistance changes by modulating the Li concentration only in the $LiCoO_2$ layer is insufficient. We designed a device to broaden the resistance change by increasing or decreasing the Li concentration in $TiO_x$, which is basically a semiconductor or insulator without Li. The direction perpendicular to the surface of $LiCoO_2/TiO_x$ is the direction of Li-ion migration. The Li-ions are made to move by applying voltage between the cathode and anode. LiPON, the Li-ion conductive layer, is a solid material that enables Li-ions to pass through but not electrons. A material with high ion conductivity is desirable for Li ions. So, amorphous LiPON is often used as a solid

electrolyte because it is stable in thin-film stacks [21], [22], [23], [24].

If there are no Li-ions in the $TiO_x$ on the anode and only Li-ions on the cathode, the overall state is a HRS because $TiO_x$ is a high-resistance material. When a positive voltage is applied to the cathode from this state, Li-ions are pushed out of the cathode and contained in the $TiO_x$ on the anode through the solid electrolyte; in the LRS. When a positive voltage (or negative voltage on the cathode) is applied to the anode, Li-ions are pushed out of the anode and back into the cathode through the solid electrolyte, resulting in a higher resistance depending on the Li content of the $LiTiO_x$ on the anode.

To fabricate the proposed device, we show our experimental methods described in the following. A thermally oxidized film, $SiO_2$, was formed on a Si substrate and the device structure was fabricated on top of it. The film stacks are, from the bottom on $Si/SiO_2$, $Ti/LiCoO_2/LiPON/Cu/Ti$ and $Ti/LiCoO_2/TiO_x/LiPON/TiO_x/Cu/Ti$. All deposition methods were sputtering: Ti, $LiCoO_2$, and Cu were deposited with the composition of the sputtering targets, $TiO_x$ was deposited by reactive sputtering of Ti in an oxygen atmosphere, and LiPON was deposited by reactive sputtering of $Li_3PO_4$ target in oxygen and nitrogen atmosphere. The amorphous LiPON was successfully formed due to appropriately tuned gas pressures of oxygen and nitrogen during the deposition. The device patterns were formed by using a metal mask during the depositions.

The microscopic device structure was evaluated by cross-sectional transmission electron microscopy (TEM). For electrical characteristics, the resistances were investigated by measuring the voltage after a constant current was applied. For evaluation as a resistance change device, DC *I-V* and write/read measurement by pulse application and STDP evaluation by time difference measurement of pulse application were performed. During the DC *I-V* measurement, the state change on the top electrode side of the device was observed through an optical microscope.

## III. DEVICE CHARACTERIZATIONS

The fabricated film structures were observed by cross-sectional TEM to confirm that the film thicknesses were as designed and to examine the crystal structure of each layer. As shown in Fig. 3, the low-magnification image shows that the thin films are uniformly layered with well-defined interfaces. For comparison with the $LiCoO_2/TiO_x/LiPON/TiO_x/Cu$, $LiCoO_2/LiPON/Cu$ is also shown together (Fig. 3(b)). The difference between the two samples was obvious regarding the interfaces shown as A, B and C. The measured thickness of LiPON is about 200 nm, thinner than that shown in reported examples of all-solid-state batteries [19], [20], [21]. Figure 4 shows that the two $TiO_x$ and LiPON films were amorphous, and $LiCoO_2$ is polycrystalline. $LiCoO_2$ is determined to be a hexagonal crystal structure by using out-of-plane X-ray diffraction and in-plane electron diffraction, where Li is known to move in and out reversibly as a layered intercalation material [18]. Furthermore, on the basis of our preliminary investigations with Energy-Dispersive X-ray spectroscopy (EDX), the

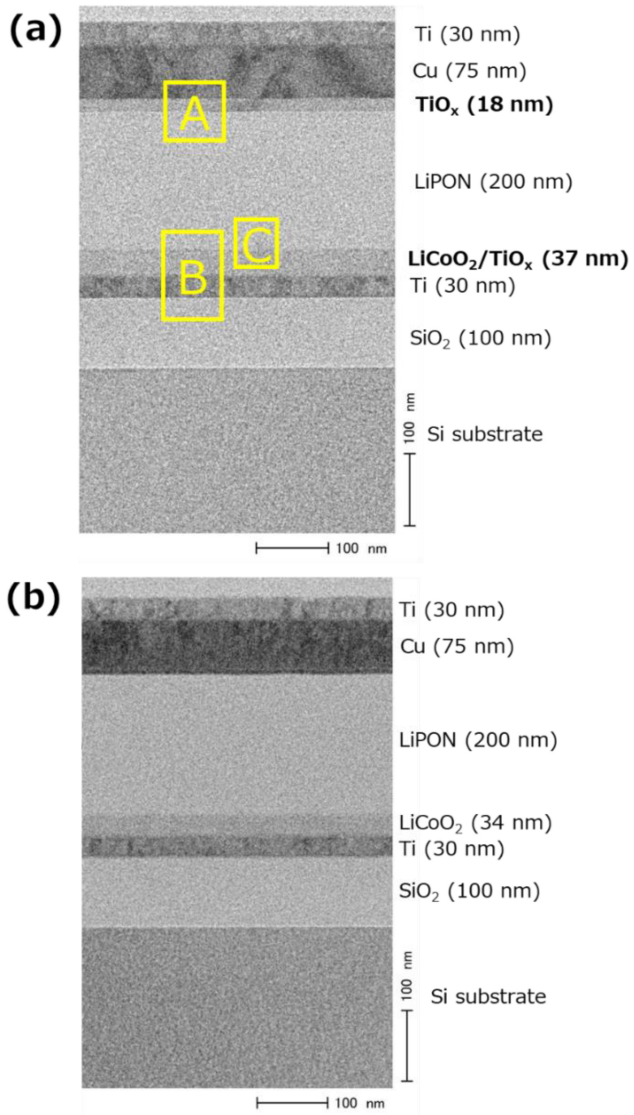


**FIGURE 3.** Cross-sectional TEM images. From the bottom layer on $Si/SiO_2$, (a) $Ti/LiCoO_2/TiOx/LiPON/TiO_x/Cu/Ti$, (b) $Ti/LiCoO_2/LiPON/Cu/Ti$.

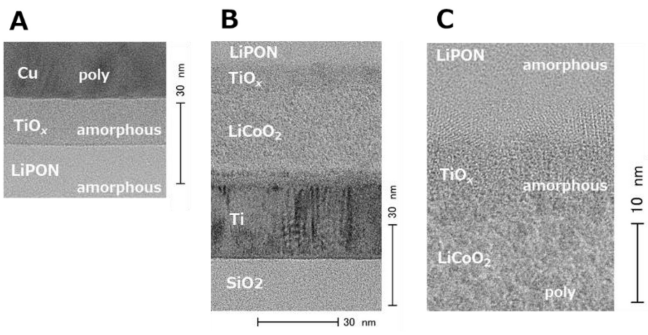


**FIGURE 4.** Enlarged cross-sectional TEM image: regions A, B, and C correspond to Fig. 3(a).

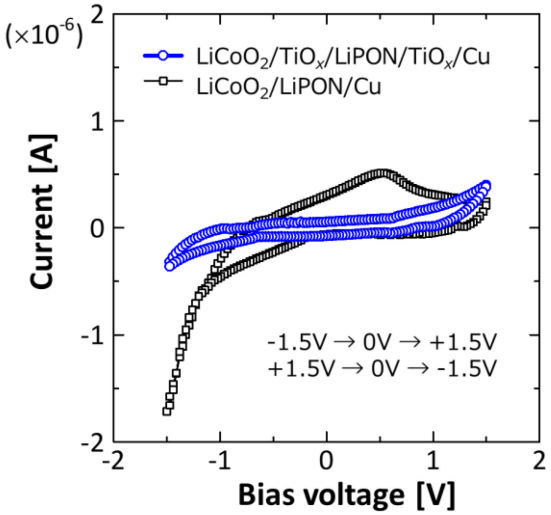


**FIGURE 5.** DC *I-V* characteristics of Ti/LiCoO$_2$/TiO$_x$/LiPON/TiO$_x$/Cu/Ti (blue circles), (b) Ti/LiCoO$_2$/LiPON/Cu/Ti (black rectangles). The device area is approximately 300 $\mu$m in diameter.

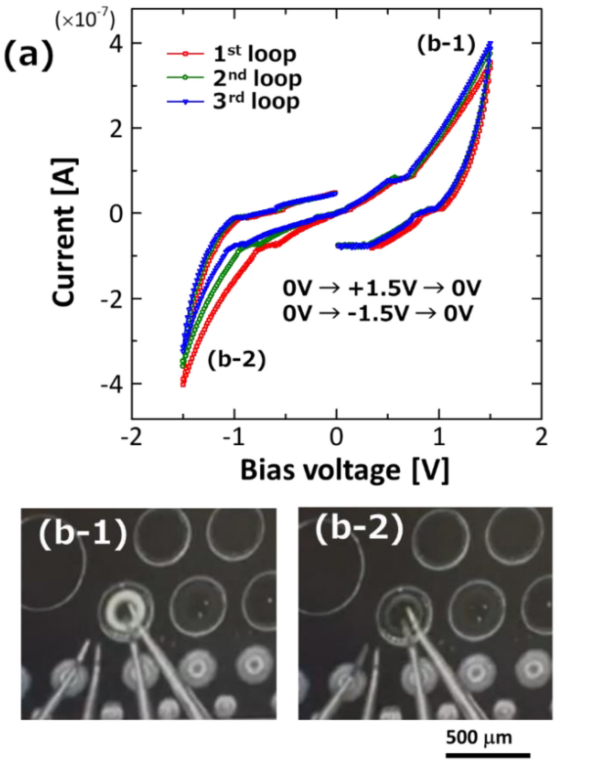


**FIGURE 6.** Measurements for LiCoO$_2$/TiO$_x$/LiPON/TiO$_x$/Cu device. (a) DC *I-V* characteristics of three loops from 0V to +1.5V and 0V to −1.5V. (b-1) and (b-2) are micrographs during operation. (b-1) is when +1V is applied and (b-2) is when −1V is applied with respect to GND (top electrode Cu/Ti), corresponding to the labeled bias conditions in (a). The device area is ∼300 $\mu$m in diameter.

presence of O atoms derived from TiO$_x$ was confirmed, indicating that the structure indeed consists of two layers of TiO$_x$ inserted at the interface between the LiCoO$_2$ and LiPON and the LiPON and Cu.

The results of the electrical evaluation are shown in the following. Figure 5 shows the *I-V* measurement results of the fabricated LiCoO$_2$/TiO$_x$/LiPON/TiO$_x$/Cu and LiCoO$_2$/LiPON/Cu. The *I-V* characteristics are hysteresis characteristics due to residual current and residual voltage. Since a positive voltage is applied to the bottom Ti/LiCoO$_2$/TiO$_x$ (cathode) on the substrate side, the top Cu/Ti (anode) was set as the ground (GND). The current gradually increases with the positive and negative biases for both samples; however, the sample with TiO$_x$ shows a lower current at the negative bias, suggesting the existence of TiO$_x$ resistivity and resulting in a more symmetric *I-V* curve with respect to the bias voltage. In contrast, the sample without TiO$_x$ shows a higher current at the negative bias and a peak current around 0.5V, suggesting a type of cyclic voltammogram of a redox system. The observed characteristic differences between the two samples suggest us that the interfacial potential difference for Li ions. Such discussion will be done at the end of this section. After more than 2V is applied, the same hysteresis curves were not always shown due to dielectric breakdown by high voltage.

Hereafter, we focus on the resistive properties of the LiCoO$_2$/TiOx/LiPON/TiO$_x$/Cu device. Figure 6(a) shows the *I-V* measurement results taken from the device of LiCoO$_2$/TiO$_x$/LiPON/TiO$_x$/Cu. The 3-loop *I-V* characteristics are hysteresis characteristics due to residual current and voltage. We found that the resistances changed loop-by-loop, under the positive biases, when less than 1.5V was applied. The current gradually increases which indicates a typical memristive property and suggests that the resistivity of TiO$_x$ decreases with Li content and the current gradually increases as Li-ions accumulate in TiO$_x$. When a positive voltage is applied to the bottom electrode, the Li concentration of the top electrode increases and the resistance decreases, which explains the decrease in resistance of the *I-V* characteristics. Similarly, when a negative voltage is applied to the bottom electrode, the Li concentration of the top electrode decreases and the resistance increases, which explains the increase in resistance of the *I-V* characteristics. Figures 6(b-1) and 6(b-2) show micrographs during the *I-V* measurements. During the measurement, a white ring-like segregation was observed on the top electrode, suggesting that Li-ions were released from LiCoO$_2$ on the bottom and reached the top. Therefore, Li-ion conduction was certainly designed as the resistance change mechanism of the neuromorphic device, and the resistance change property was demonstrated.

When the current is stopped after a certain current is applied, a residual voltage is generated. This device of LiCoO$_2$/TiO$_x$/LiPON/TiO$_x$/Cu also behaves as an all solid-state battery, although the electromotive force are not high enough for battery applications. As shown in Fig. 7, the voltage after current pulsing stops exponentially decreased due to the release of charge stored in capacitance *C* through the resistance *R* of the internal device. After a certain time, the residual voltage settles at about 0.7V, and it is maintained and then gradually decreases. A circuit model can be

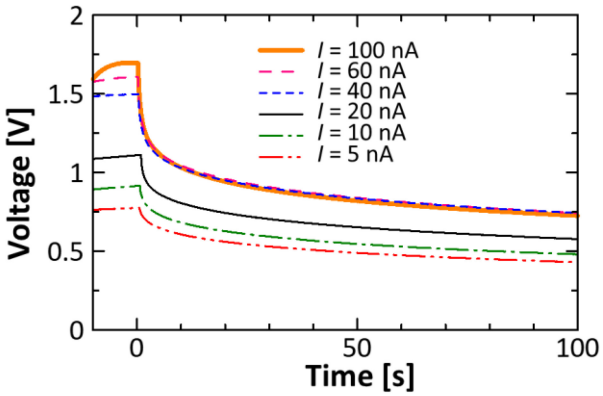


**FIGURE 7.** Residual voltages in $LiCoO_2/TiO_x/LiPON/TiO_x/Cu$ device. Constant currents ($I$ = 5, 10, 20, 40, 60, 100 nA) were applied up to 0 s, then the residual voltages were measured as a function of time. The device area is approximately 300 $\mu$m in diameter.

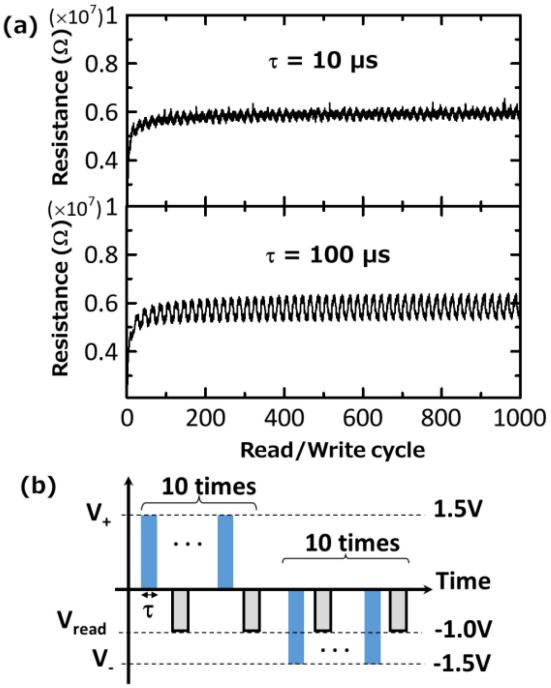


**FIGURE 8.** Repeated resistance measurement. (a) Write 10 times each cycle to change to the same polarity, and read each time after write. From top to bottom, write pulse widths ($\tau$) are 10 $\mu$s and 100 $\mu$s. The device area is ~300 $\mu$m in diameter. (b) the pulse measurement setup with write pulse $V_+$ (+1.5V) and $V_-$ (−1.5V) and read voltage $V_{read}$ (−1.0V).

drawn in which $R$ and $C$ are in parallel and the charging voltage $V$, i.e., electromotive force, is also in series. If the current pulsing time for charging is too short or the current is small ($I$ = 5, 10, 20 nA), the residual voltage tends to be less than 0.7V. So, the multi-level residual voltage can be controlled by the applied current. However, those observed voltage characteristics are not our main target of the fabricated device with $LiCoO_2/TiO_x/LiPON/TiO_x/Cu$, but resistive characteristics in the following.

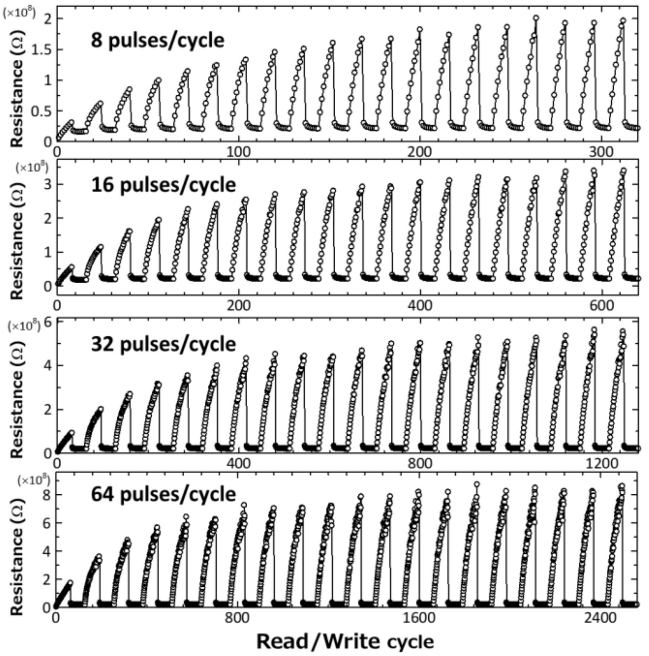


**FIGURE 9.** Evaluation of multi-level values by repeated resistance measurement. Writing in the direction of increasing resistance, we examined whether it can be decomposed into 8, 16, 32, and 64 values each. The device area is ~200 $\mu$m in diameter.

The repeated resistance change characteristics were then examined. In Fig. 8, the vertical axis is the read resistance, and the horizontal axis is the number of write/read cycles. The repetition of resistance changes in response to pulse voltage can be clearly seen. However, the battery-type device ($LiCoO_2$/LiPON/Cu) measured for comparison does not exhibit clear repetitive resistance changes. In the measurement, write pulses were given about 10 times with one voltage polarity, read out each time, and then the set was repeated many times by switching the polarity (Fig. 9(b)). In the results shown in the figure, the write pulse width ($\tau$) was evaluated by changing the orders of 10 $\mu$s and 100 $\mu$s. Depending on $\tau$, the resistance change differs due to the inherent time constant of the device.

Next, as shown in Fig. 9, the pulse width ($\tau$) was fixed at 200 $\mu$s and the resistance value was varied to one side (in this case, in the direction of increasing resistance) asymmetrically to examine the change in resolution of the resistance memory value. The device seems to have both short- and long-term plasticity, and the resistance appears to be waking up gradually with repeated pulses. The resolution was judged to have been obtained if the resistance value could be separated for each pulse number, and a memory resolution of 32 values was found as shown in the middle of the figure. The obtained multi-level resistance changes in the two terminal device are comparable with previously reported Li-ion based three terminal devices [22], [23], [24]. As a result, the demonstrated device is a new type of memristor that changes the distribution of Li-ions in the device by electrolysis to achieve an LRS and an HRS. Conventional

memristors have a structure with metal electrodes such as $TiO_2$ at both ends and use oxygen deficiency with low charge mobility as a material for resistance control, making it difficult to maintain stable LRSs and HRSs. Variations and fluctuations in the properties of each element become large. In contrast, since Li-ions have greater mobility than oxygen defects, they are expected to be more uniform in annealing during fabrication and migration by electric fields, and thus reduce the resistance variation of each element, which is important for memristor applications. Sixty-four values shown at the bottom in Fig. 9 would cause an overlap in the resistance change which is not good enough to distinguish each resistance in practical uses. Since the behavior differs between the early and late stages of read and write operations, further device structures and evaluation methods need to be investigated to improve the memory resolution in the future.

There is an upper limit to the amount of the Li-ions charge in the cathode layer. Therefore, when using this device, it is necessary to control the drive circuit and devise the read/write operation so that the upper limit of the current integration for readout is not exceeded. One method is to use positive and negative bipolar pulses, such as STDP evaluation. By using this method, the net migration of Li ions should be always the same, so many readouts can be continued in the same state. Figure 10 shows the STDP results of conductance changes for our $LiCoO_2/TiO_x/LiPON/TiO_x/Cu$ device. In this study, a new shape of the STDP curve were determined to be a hyperbolic tangent (tanh) function-shape, which is contrast with our previous result in memristive devices of metal-oxides [30]. The tanh shape was obtained because, first, the conductance change saturates and becomes constant when the timing is far enough apart because it is determined by the sensitivity of the element to the pulse intensity and time width. Second, because one spike effectively reduces the intensity of the other spike near zero-time difference where the pulses overlap. This newly observed curve is considered for some specific neuromorphic computing, e.g., reservoir computing, described in the next section. Although more detailed analysis is needed, STDP is one useful feature for various learning rules for autonomous and local synapse value updates.

Here, we further discuss the device properties. The demonstrated device is a multilayer film composed of a conductor and an insulator. For the respective charge carriers of Li ions and electrons flowing in the device, the potential felt at the interface is not simple. We consider a Schottky barrier between the insulator or semiconductor and the ionic conductor, respectively: for Li ions, there is the bulk ion conductivity in the solid electrolyte and the interface resistivity at the interface between the solid electrolyte and the electrode. In fact, the bulk resistivity alone cannot explain the resistance of the stacked structure. Since the design concept of this device aims at linearly varying the resistance by controlling the bulk resistivity, the interface resistance should be as small as possible. Interfacial resistance is often

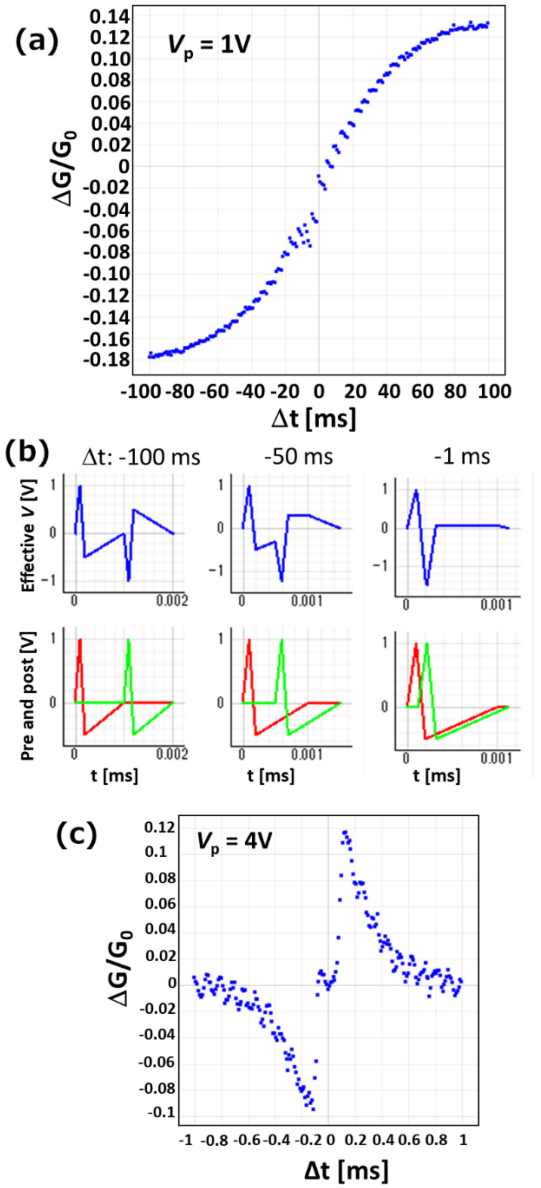


**FIGURE 10.** Spike-Timing Dependent Plasticity (STDP) measurement results taken from $Ti/LiCoO_2/TiO_x/LiPON/TiO_x/Cu/Ti$. (a) hyperbolic tangent (tanh)-type timing difference dependence is observed. The device area is ~200 $\mu$m in diameter. (b) This result depends on how the spike waveform shape is given and the range of timing magnitude. (c) typical conventional STDP characteristics shown in our previous devices, $WO_x$/MgO/TiN for comparison [30].

sensitive to structure, and previous studies of Li-ion batteries have shown that interfacial resistance depends on the cleanliness of the interface, crystallinity of the solid electrolyte, and orientation of the cathode and anode [33], [34], [35], [36]. Schottky-type interfacial resistance, which depends on the difference between the Fermi level of the electrode such as $LiCoO_2$ and the Fermi level of the Li-ion conducting layer such as LiPON, is also influential. Those considerations are not in the scope of this study but for future works.

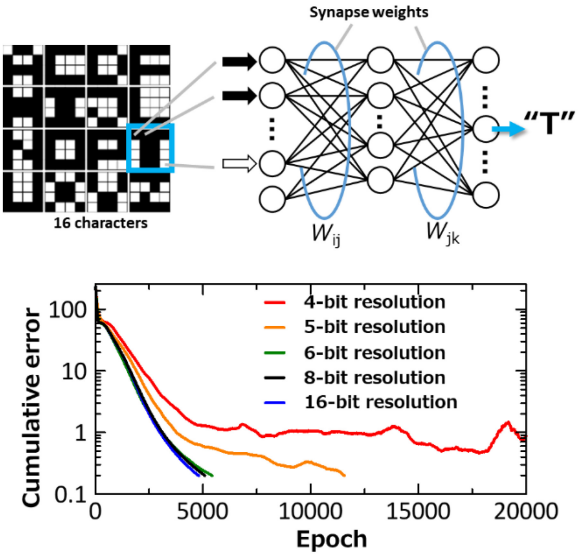


**FIGURE 11.** 3-layer NN and learning performance with reduced weight resolutions. 16 characters of 16 pixels were used for the learning. The resolutions of $W_{ij}$ and $W_{jk}$ were down from 16 to 4 bit.

## IV. ANALYSIS ON NEUROMORPHIC COMPUTING APPLICATIONS

Since the device works with long- and short-term memory, the long-term memory is the change in resistance of $TiO_x$ due to the operation of Li ions. As shown in the figure, the analog value changes and the memory is fixed in this operating range. The problem is that the *I-V* characteristics are highly nonlinear, so the readout method must also be considered, in which –1.5V was used for a trial, however the detailed analysis is beyond the scope of this paper. Figures 11 and 12 show simulation results that provide a glimpse into the future and are based on several assumptions. The device memory is long enough, and the weight values do not change after being written. Although these are difficult to achieve in a real device, it is indicated that there are applications where even a low resistance resolution of about 32 values can be used.

From previous studies and CMOS circuit designs, an analog memory device using a capacitor yields 200-300 distinguished steps, i.e., an 8-bit resolution equivalent in digital [6]. Here, we show by analysis on two types of NN learning considering synaptic weights of an 8-bit resolution or less are used.

Figure 11 shows the results of learning with the back propagation method, assuming a typical 3-layer feedforward NN for 16 characters of 16 pixels that can be operated with our previously-developed analog neuromorphic circuit [30]. The simulation in Figure 11 is a numerical simulation assuming 16, 32, 64, 256 and 65536 values (4-, 5-, 6-, 8- and 16-bit equivalent), rather than using the actual device resistance (experimental data, e.g., for 32-value operation) to estimate the cumulative error. In this recognition application, if the cumulative error in learning can be sufficiently small, the recognition accuracy is almost 100%. When the precision of the weights, $W_{ij}$ and $W_{jk}$, is reduced from 32 bit to 16, 8, and 6 bit, there is almost no change up to 6 bit, and from 5 bit, the number of learning cycles to convergence increases, and convergence is not achieved at 4 bit. In other words, in this example, a 5-bit resolution (32 values) is good enough for this NN.

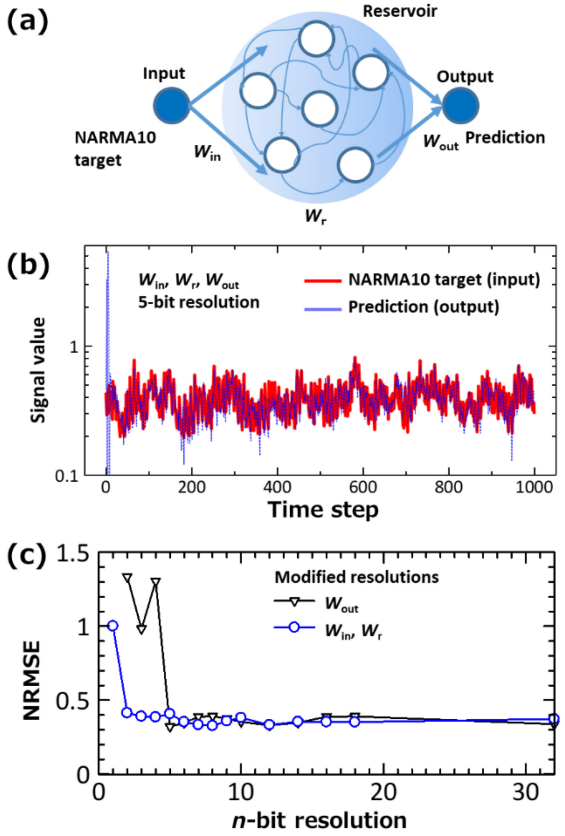


**FIGURE 12.** Reservoir computing (RC) analysis. (a) a RC model with echo state networks (ESNs). (b) Simulation example of ESN and NARMA10 under the condition of reduced weight resolutions. (c) Summarized results of NARMA10 benchmark to determine the least resolutions required to obtain sufficient performance, i.e., appropriately high normalized root-mean-square error (NRMSE).

Brain-inspired algorithms tend to outperform conventional machine learning at processing time-series data. For such time-series data, reservoir computing (RC) has been intensively studied, which uses random weights in the reservoir and does not change the weight value during training or learning, and the nonlinearly transformed signals in the reservoirs are extracted from the outputs. Only the weights between the reservoir and the output are updated during learning before inference. Since the weight update amount is quite small, the RC learning can be finished sooner than other recurrent NNs [37], [38]. The most commonly used RC is the echo state network (ESN), in which the connections between neurons are sparse and random, and the firing of neurons is represented by a nonlinear function. If the state of a neuron in the reservoir is $R$[t], the neuron at time t→t+1 is

$$R[\mathrm{t}+1] = (1-\alpha)R[\mathrm{t}] + \alpha \tanh([1, \mathrm{data}[\mathrm{t}+1]] \times W_{\mathrm{in}}) + R[\mathrm{t}] \times W_{\mathrm{r}} \quad (1)$$

where $\alpha$ is the decay parameter, 40-80%. The forgotten value is updated from the new input data and nonlinearized by the tanh function. At the same time, it is affected by the results of the sum-of-products operation from other neurons.

A typical benchmark for the reservoir is a nonlinear function called Nonlinear Autoregressive Moving Average (NARMA) 10 [39], [40]. The more neurons in the reservoir, the better the performance; however, it will also become more computationally heavy and time-consuming. NARMA10 needs a one-input, one-output nonlinear time-series pattern. The number of nodes or neurons in the reservoir is 100, and the recursive connection rate in the reservoir is 80%. These are not special conditions, but simulation results based on generally used conditions for RC benchmarks. Figure 12 shows the results of reducing the weight resolution during training or learning for the input-to-reservoir weights $W_{in}$ and the intra-reservoir weights $W_r$. There is almost no change up to a 5-bit resolution, and interestingly, even a 2-bit resolution remain usable. Although 2 bit is 4 values, it is thought that it can be reduced to three values (negative, near zero, and positive) in practice. However, Fig. 12 also shows the results of reducing the resolutions of the weight $W_{out}$ between the reservoir and output, which does not change up to about a 5-bit resolution, but the performance degrades noticeably below a 4-bit resolution. In the aforementioned RC example, about 5 bits is likely to be sufficient for the accuracy of the synaptic weights during training. Therefore, this analysis also confirms that the 32 values of 5-bit resolution, which was demonstrated in the $LiCoO_2/TiO_x$/LiPON/$TiO_x$/Cu device of this study, is sufficient to explore RC applications. This device is used for weights in the reservoir calculation; with a resolution of 32 values, the performance of the run is not much degraded after learning, so it can be used to predict signals like NARMA10 in the example. It can also be used for dynamic and nonlinear response of the reservoir section. Since it depends on the size of the NN, it is necessary to verify it for various applications including exciting physical RC with nonlinear devices [41], [42], [43]. Taking into consideration experimentally observed multi-value resistances and a novel STDP function similar to tanh, the proposed and demonstrated Li-based resistive devices have great potential to be a key device component in neuromorphic computing in a new era.

## V. CONCLUSION

In this study, we investigated the feasibility of resistance change devices by Li-ion conduction by combining $LiCoO_2$, which is used as a positive electrode material in Li-ion batteries, and thin films of solid electrolytes used in all-solid-state batteries. The results showed that $LiCoO_2$/LiPON/Cu can be fabricated by sputtering deposition with good affinity to semiconductor processes. Li-ion conduction was designed as a resistance change mechanism for neuromorphic devices, and its resistance change properties were demonstrated. In particular, we inserted ultrathin titanium-dioxide films at the interface and clarified the resistance change and then discussed its effect on the resistance change properties. It was experimentally demonstrated that Li-based ionic conduction provides plasticity as a neuromorphic two-terminal synaptic device, and further analysis showed that its resistance change properties are promising for opening new neuromorphic applications.

## REFERENCES

[1] G. E. Hinton and R. R. Salakhutdinov, "Reducing the dimensionality of data with neural networks," *Science*, vol. 313, no. 5786, pp. 504–507, Jul. 2006, doi: 10.1126/science.1127647.
[2] Y. LeCun, Y. Bengio, and G. Hinton, "Deep learning," *Nature*, vol. 521, pp. 436–444, May 2015, doi: 10.1038/nature14539.
[3] C. D. Schuman, S. R. Kulkarni, M. Parsa, J. P. Mitchell, P. Date, and B. Kay, "Opportunities for neuromorphic computing algorithms and applications," *Nat. Comput. Sci.*, vol. 2, pp. 10–19, Mar. 2022, doi: 10.1038/s43588-021-00184-y.
[4] A. Mehonic and A. J. Kenyon, "Brain-inspired computing needs a master plan," *Nature*, vol. 604, pp. 255–260, Apr. 2022, doi: 10.1038/s41586-021-04362-w.
[5] N. Qiao et al., "A reconfigurable on-line learning spiking neuromorphic processor comprising 256 neurons and 128K synapses," *Front. Neurosci.*, vol. 9, p. 141, Apr. 2015, doi: 10.3389/fnins.2015.00141.
[6] H. Tsai, S. Ambrogio, P. Narayanan, R. M. Shelby, and G. W. Burr, "Recent progress in analog memory-based accelerators for deep learning," *J. Phys. D, Appl. Phys.*, vol. 51, no. 28, Jun. 2018, Art. no. 283001, doi: 10.1088/1361-6463/aac8a5.
[7] E. Chicca and G. Indiveri, "A recipe for creating ideal hybrid memristive-CMOS neuromorphic processing systems," *Appl. Phys. Lett.*, vol. 116, Mar. 2020, Art. no. 120501, doi: 10.1063/1.5142089.
[8] W. Banerjee, R. D. Nikam, and H. Hwang, "Prospect and challenges of analog switching for neuromorphic hardware," *Appl. Phys. Lett.*, vol. 120, Feb. 2022, Art. no. 60501, doi: 10.1063/5.0073528.
[9] W. Wang et al., "Physical based compact model of Y-Flash memristor for neuromorphic computation," *Appl. Phys. Lett.*, vol. 119, Dec. 2021, Art. no. 263504, doi: 10.1063/5.0069116.
[10] V. Kurtash, S. Thiele, S. Mathew, H. O. Jacobs, and J. Pezoldt, "Designing $MoS_2$ channel properties for analog memory in neuromorphic applications," *J. Vac. Sci. Technol. B*, vol. 40, Apr. 2022, Art. no. 30602, doi: 10.1116/6.0001815.
[11] S. Ambrogio et al., "Equivalent-accuracy accelerated neuralnetwork training using analogue memory," *Nature*, vol. 558, p. 7, Jun. 2018, doi: 10.1038/s41586-018-0180-5.
[12] I. Boybat et al., "Neuromorphic computing with multi-memristive synapses," *Nat. Commun.*, vol. 9, p. 2514, Jun. 2018, doi: 10.1038/s41467-018-04933-y.
[13] S. X. Go, T. H. Lee, S. R. Elliott, N. Bajalovic, and D. K. Loke, "A fast, low-energy multi-state phase-change artificial synapse based on uniform partial-state transitions," *APL Mater.*, vol. 9, Sep. 2021, Art. no. 91103, doi: 10.1063/5.0056656.
[14] Z. Wang et al., "Compact modelling of ferroelectric tunnel memristor and its use for neuromorphic simulation," *Appl. Phys. Lett.*, vol. 104, Feb. 2014, Art. no. 53505, doi: 10.1063/1.4864270.
[15] R. Berdan et al., "Low-power linear computation using nonlinear ferroelectric tunnel junction memristors," *Nat. Electr.*, vol. 3, no. 5, p. 259, May 2020, doi: 10.1038/s41928-020-0405-0.
[16] H. Yeon et al., "Alloying conducting channels for reliable neuromorphic computing," *Nat. Nanotech.*, vol. 5, p. 574, Jun. 2020, doi: 10.1038/s41565-020-0694-5.
[17] J. Ma et al., "The 2021 battery technology roadmap," *J. Phys. D, Appl. Phys.*, vol. 54, Feb. 2021, Art. no. 183001, doi: 10.1088/1361-6463/abd353.
[18] K. Mizushima, P. C. Jones, P. J. Wiseman, and J. B. Goodenough, "LixCoO2 (0<x<-1): A new cathode material for batteries of high energy density," *Mater. Res. Bull.*, vol. 15, no. 6, pp. 783–789, Jun. 1980, doi: 10.1016/0025-5408(80)90012-4.
[19] Y. Kato et al., "High-power all-solid-state batteries using sulfide superionic conductors," *Nat. Eneg.*, vol. 1, Apr. 2016, Art. no. 16030, doi: 10.1038/NENERGY.2016.30.

[20] C. Chen et al., "Interface aspects in all-solid-state Li-based batteries reviewed," *Adv. Energy Mater.*, vol. 11, Apr. 2021, Art. no. 2003939, doi: 10.1002/aenm.202003939.
[21] B. J. Neudecker, N. J. Dudney, and J. B. Bates, "'Lithium-free' thin-film battery with *In Situ* plated Li anode," *J. Electrochem. Soc.*, vol. 147, no. 2, pp. 517–523, 2000, doi: 10.1149/1.1393226.
[22] E. J. Fuller et al., "Li-ion synaptic transistor for low power analog computing," *Adv. Mater.*, vol. 29, Nov. 2017, Art. no. 1604310, doi: 10.1002/adma.201604310.
[23] T. Tsuchiya et al., "The electric double layer effect and its strong suppression at Li+ solid electrolyte/hydrogenated diamond interfaces," *Commun. Chem.*, vol. 4, p. 117, Aug. 2021, doi: 10.1038/s42004-021-00554-7.
[24] X. Wan, T. Tsuruoka, and K. Terabe, "Neuromorphic system for edge information encoding: Emulating retinal center-surround antagonism by Li-ion-mediated highly interactive devices," *Nano Lett.*, vol. 21, pp. 7938–7945, Sep. 2021, doi: 10.1021/acs.nanolett.1c01990.
[25] W. Gerstner, R. Ritz, and J. L. Hemmen, "Why spikes? Hebbian learning and retrieval of time-resolved excitation patterns," *Biol. Cybern.*, vol. 69, pp. 503–515, Oct. 1993, doi: 10.1007/BF00199450.
[26] G. Bi and M. Poo, "Synaptic modifications in cultured hippocampal neurons: Dependence on spike timing, synaptic strength and postsynaptic cell type," *J. Neurosci.*, vol. 18, pp. 10464–10472, Dec. 1998, doi: 10.1523/JNEUROSCI.18-24-10464.1998.
[27] S. H. Jo, T. Chang, I. Ebong, B. B. Bhadviya, P. Mazumder, and W. Lu, "Nanoscale memristor device as synapse in neuromorphic systems," *Nano Lett.*, vol. 10, p. 1297, Apr. 2010, doi: 10.1021/nl904092h.
[28] G. Indiveri et al., "Neuromorphic silicon neuron circuits," *Front. Neurosci.*, vol. 5, p. 73, May 2011, doi: 10.3389/fnins.2011.00073.
[29] T. Marukame, Y. Nishi, S.-I. Yasuda, and T. Tanamoto, "Artificial neuron operations and spike-timing-dependent plasticity using memristive devices for brain-inspired computing," *Jpn. J. Appl. Phys.*, vol. 57, no. 4S, Mar. 2018, Art. no. 4FK06, doi: 10.7567/JJAP.57.04FK06.
[30] T. Marukame et al., "Integrated analog neurons inspired by mimicking synapses with metal-oxide memristive devices," *Jpn. J. Appl. Phys.*, vol. 59, Apr. 2020, Art.no. 40606, doi: 10.35848/1347-4065/ab8164.
[31] Y. Nishi, K. Nomura, T. Marukame, and K. Mizushima, "Stochastic binary synapses having sigmoidal cumulative distribution functions for unsupervised learning with spike timing-dependent plasticity," *Sci. Rep.*, vol. 11, Sep. 2021, Art. no. 18282, doi: 10.1038/s41598-021-97583-y.
[32] M. Payvand, F. Moro, K. Nomura, T. Dalgaty, and E. Vianello, "Self-organization of an inhomogeneous memristive hardware for sequence learning," *Nat. Commn.*, vol. 13, p. 5793, Sep. 2022, doi: 10.1038/s41467-022-33476-6.
[33] N. Ohta, K. Takada, L. Zhang, R. Ma, M. Osada, and T. Sasaki, "Enhancement of the high-rate capability of solid-state lithium batteries by nanoscale interfacial modification," *Adv. Mater.*, vol. 18, pp. 2226–2229, May 2006, doi: 10.1002/adma.200502604.
[34] M. W. Swift, J. W. Swift, and Y. Qi, "Modeling the electrical double layer at solid-state electrochemical interfaces," *Nat. Comput. Sci.*, vol. 1, pp. 212–220, Mar. 2021, doi: 10.1038/s43588-021-00041-y.
[35] B. Put, P. M. Vereecken, and A. Stesmans, "On the chemistry and electrochemistry of LiPON breakdown," *J. Mater. Chem. A*, vol. 6, p. 4848, Feb. 2018, doi: 10.1039/c7ta07928a.
[36] S. Shiraki, T. Shirasawa, T. Suzuki, H. Kawasoko, R. Shimizu, and T. Hitosugi, "Atomically well-ordered structure at solid electrolyte and electrode interface reduces the interfacial resistance," *ACS Appl. Mater. Interfaces*, vol. 10, no. 48, pp. 41732–41737, Nov. 2018, doi: 10.1021/acsami.8b08926.
[37] H. Jaegar and H. Haas, "Harnessing nonlinearity: Predicting chaotic systems and saving energy in wireless communication," *Science*, vol. 304, pp. 78–80, Apr. 2004, doi: 10.1126/science.1091277.
[38] G. Tanaka et al., "Recent advances in physical reservoir computing: A review," *Neural Netw.*, vol. 115, pp. 100–123, Jul. 2019, doi: 10.1016/j.neunet.2019.03.005.
[39] A. F. Atiya and A. G. Parlos, "New results on recurrent network training: Unifying the algorithms and accelerating convergence," *IEEE Trans. Neural Netw.*, vol. 11, no. 3, pp. 697–709, May 2000, doi: 10.1109/72.846741.
[40] T. Kanao, H. Suto, K. Mizushima, H. Goto, T. Tanamoto, and T. Nagasawa, "Reservoir computing on spin-torque oscillator array," *Phys. Rev. Appl.*, vol. 12, Aug. 2019, Art. no. 24052, doi: 10.1103/PhysRevApplied.12.024052.
[41] C. Du, F. Cai, M. A. Zidan, W. Ma, S. H. Lee, and W. D. Lu, "Reservoir computing using dynamic memristors for temporal information processing," *Nat. Commn.*, vol. 8, p. 2204, Dec. 2017, doi: 10.1038/s41467-017-02337-y.
[42] H. Tanaka et al., "A molecular neuromorphic network device consisting of single-walled carbon nanotubes complexed with polyoxometalate," *Nat. Commn.*, vol. 9, p. 2693, Jul. 2018, doi: 10.1038/s41467-018-04886-2.
[43] K. Ota, M. Yamaguchi, S. Kabuyanagi, S. Fujii, M. Saitoh, and M. Yoshikawa, "Variability-controlled HfZrO2 ferroelectric tunnel junctions for reservoir computing," *IEEE Trans. Electron Devices*, vol. 69, no. 12, pp. 7089–7095, Dec. 2022, doi: 10.1109/TED.2022.3212332.

**TAKAO MARUKAME** (Member, IEEE) was born in Sapporo, Japan, in 1978. He received the B.E. and M.E. degrees in engineering and the Dr. (Eng.) degree in information science and technology from Hokkaido University, Hokkaido, Japan, in 2002, 2004, and 2007, respectively.

Since 2007, he has been with Toshiba Corporation, Kawasaki, Japan, where he has engaged in research on advanced LSI technology, spintronic devices, and memory systems. From 2014 to 2015, he was a Visiting Scientist with Ecole Polytechnique Federale Lausanne, Lausanne, Switzerland, where he studied microelectronic circuits and systems. He is currently working on the development of neuromorphic and brain-inspired devices. He is a member of the Japan Society of Applied Physics.

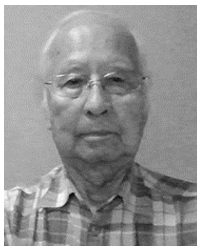

**KOICHI MIZUSHIMA** received the B.S., M.S., and Ph.D. degrees in solid state physics from Tokyo University in 1964, 1966, and 1969, respectively.

From 1964 to 1981, he was with Tokyo University, where he did mainly basic researches concerning magnetostriction, hopping-conduction and metal/insulator transitions in transition-metal oxides. In 1978 and 1979, he was with Inorganic Chemistry Laboratory, Oxford, and developed new cathode-materials for secondary lithium-batteries. From 1982 to 2018, he was with Research and Development Center, Toshiba Corporation, Kawasaki, Japan, where he has done various researches, such as molecular electronics using Langmuir-Blodgett films, high-temperature superconducting devices, spin-valve transistors, and spin-transfer microwave nano-oscillators applied to magnetic recording heads. Since 2019, he has been developing hardware for neuromorphic neural networks.

**KUMIKO NOMURA** received the B.E. degree in information Science and the M.E. and Dr.(Eng.) degrees in communications and integrated systems from the Tokyo Institute of Technology, Tokyo, Japan, in 2000, 2002, and 2005, respectively. Since 2005, she has been with Toshiba Corporation, Kawasaki, Japan, where she has engaged in research on advanced LSI technology systems. She is currently working on the development of neuromorphic and brain-inspired systems. She is a member of the Institute of Electronics, Information and Communication Engineers.

**YOSHIFUMI NISHI** received the B.S., M.S., and Ph.D. degrees in physics from the University of Tokyo, Tokyo, Japan, in 2000, 2002, and 2005, respectively.

Since 2005, he has been with Toshiba Corporation, Kawasaki, Japan, where he has engaged in research on advanced LSI technology, silicon devices and memory systems. From 2012 to 2013, he was a Visiting Scientist with RWTH Aachen University, Aachen, Germany, where he studied the resistive switching devices. He is currently working on the development of neuromorphic and brain-inspired devices and systems. He is a member of the Japan Society of Applied Physics.